Radiative impact of the Hunga Tonga-Hunga Ha'apai stratospheric volcanic plume: role of aerosols and water vapor in the southern tropical Indian Ocean

M. Sicard[1,2], A. Baron[3], M. Ranaivombola[1], D. Gantois[1], T. Millet[1], P. Sellitto[4], N. Bègue[1], G. Payen[5], N. Marquestaut[5], and V. Duflot[1]

[1]Laboratoire de l'Atmosphère et des Cyclones (LACy), UMR 8105 CNRS, Université de La Réunion, Météo-France, Saint-Denis de la Réunion, France

[2]CommSensLab-UPC, Universitat Politècnica de Catalunya, Barcelona, Spain

[3]Cooperative Institute for Research in Environmental Sciences, and NOAA Chemical Sciences Laboratory, Boulder, USA

[4]Laboratoire Interuniversitaire des Systèmes Atmosphériques (LISA-IPSL), Institut Pierre Simon Laplace, Université Paris-Est Créteil and Université de Paris-Cité, CNRS, Créteil, France

[5]Observatoire des Sciences de l'Univers – Réunion (OSU-R), Saint Denis, France

Corresponding author: Michaël Sicard (michael.sicard@univ-reunion.fr)

Key Points:

- One year after HTHH eruption, aerosols and water vapor from the volcano are still present in the stratosphere
- The aerosol plume has decayed with time, while the moist layer ascended
- The descending rate of the volcanic plume is -0.008 km day^{-1}; at this rate, aerosols will remain in the stratosphere until mid-2025
- So far, aerosols and WV have contributed to warm the Earth-Atmosphere system in the southern tropical Indian Ocean (+0.06 ± 0.45 W m-2)

Abstract

This study attempts to quantify the radiative impact over Reunion Island (21°S, 55°E) in the southern tropical Indian Ocean of the aerosols and water vapor injected in the stratosphere by the eruption on 15 January 2022 in the South Pacific of the Hunga Tonga-Hunga Ha'apai underwater volcano. Ground-based lidar and satellite passive instruments are used to parametrize a state-of-the-art radiative transfer model for the first thirteen months after the volcano eruption. The descending rate of the aerosol volcanic plume is -0.008 km day^{-1}. At this rate, aerosols are expected to be present in the stratosphere until the first half of 2025. The overall aerosol and water vapor impact on the Earth's radiation budget for the whole period is positive (warming, +0.06 ± 0.45 W m^{-2}) and dominated by the aerosol impact. However, the decreasing rate with time of the aerosol warming effect is larger than that of the water vapor cooling effect, so that, in the long run, the impact on the Earth's radiation budget might reduce to quasi-neutral, or even become slightly negative. At the Earth's surface, aerosols are the main driver and produce a negative (cooling, -0.91 ± 0.61 W m^{-2}) radiative impact with also a decreasing tendency with time. Heating/cooling rate profiles show a clear vertical difference in the stratosphere between the aerosol warming impact (17 to 25 km) and the water vapor cooling one (25 to 40 km).

1 Introduction

More than one year and a half after the eruption of Hunga Tonga-Hunga Ha'apai (HTHH) underwater volcano in the South Pacific, the science community is still actively investigating the climate impact of the huge amounts of ash, water, steam and gases that were injected in the atmosphere. The event showed an extremely fast spatio-temporal, global dispersion of the stratospheric volcanic matter that circulated the Earth in only one week (Khaykin et al., 2022) and diluted pole-to-pole in three months (Taha et al., 2022), not simply passively but rather organized in concentrated patches (Legras et al., 2022). Several figures are evidences of a record-breaking atmospheric event. The eruption, equivalent to an energy of 110 Tg of TNT, is the most powerful volcanic explosion since Krakatau (1883) and Tambora (1815) (Lac et al., 2022). The volcanic plume reached an altitude of 57 km, a coincident estimation resulting from different techniques (Carr et al., 2022; Proud et al., 2022), placing it in the upper stratosphere – lower mesosphere, a record in the satellite era. The water injected was unprecedented: (Millán et al., 2022) estimated to 146 Tg the mass of water injected in the atmosphere (.e.g. the 1991 Pinatubo eruption released 37 Tg of water into the atmosphere (Pitari & Mancini, 2002)). In contrast, sulfur dioxide (SO_2) mass injection was not that exceptional: ~ 0.6 – 0.7 Tg (Carn et al., 2022) which is much smaller than that from previous major eruptions (e.g. 20 Tg for Pinatubo (Bluth et al., 1992)). Still, the stratospheric aerosol optical depth (sAOD) has been recorded as the largest since Pinatubo eruption (Taha et al., 2022) and peaked at values never observed before (Baron et al., 2023).

The latter three variables (water, SO_2 and injection height) are some of the main factors responsible for the production of volcanic sulfate and for the loss/production of ozone. The initial SO_2 was fully converted into sulfates in less than two weeks under the influence of water vapor (Asher et al., 2022; Legras et al., 2022), whereas volcanic sulfate and water still persist as of today. The fast water vapor injection provided abundant hydroxide (OH) which reacted with SO_2 to form volcanic sulfate at a faster rate than the typical ~ 30 days. Higher concentrations of volcanic sulfate led to more rapid coagulation and thus larger particles. In the case of HTHH, this mechanism is estimated to have halved the SO_2 lifetime and doubled the sAOD (Zhu et al., 2022). This rapid growth and global persistence of volcanic sulfate aerosols have been demonstrated with

AERONET measurements by (Boichu et al., 2023) with the occurrence of an unusual "volcanic fine mode" with a peak ranging in 0.28 – 0.50 μm. This fine mode was found to be poorly absorbing, although (Kloss et al., 2022) reports from balloon-borne measurements a moderately absorbing fine mode in the first 10 days after the eruption indicating small sulfate coated ash particles. Volcanic sulfate is known to be a factor to impact ozone depletion by providing additional surface area and suppressing the nitric oxide cycle (Tie & Brasseur, 1995). The transport of volcanic sulfate from the tropics to the Antarctic by the Brewer-Dobson circulation contributed to increase ozone concentrations in the middle stratosphere but to decline in the lower stratosphere at mid-to-low latitudes (Lu et al., 2023), while, combined with a cold polar vortex, it contributed to decrease ozone concentration in the Antarctic (Wang et al., 2022). Because ozone is not emitted primarily during volcanic eruptions, its loss or production by post-eruption reactions are more tedious to estimate. The effect of HTHH on stratospheric ozone is still under study.

Water, volcanic sulfate and the injection height are the main drivers of the impact of HTHH on atmospheric global circulation (Coy et al., 2022) and climate (Zuo et al., 2022). In particular, the climate forcing will depend on the radiative effect produced by the water vapor longwave emission and the aerosol shortwave and longwave scattering and absorbing properties. These interaction mechanisms (emission, scattering and absorption) with the shortwave and longwave radiation are highly height-dependent and determine the sign of the differential of energy gained (positive) or lost (negative) in all layers of the atmosphere. Several studies have demonstrated the stratospheric cooling produced by the excess of water vapor injected by HTHH either locally (Sellitto et al., 2022), zonally (Schoeberl et al., 2022; Vömel et al., 2022; Zhu et al., 2022) or globally (Millán et al., 2022) at different time scales spanning from instantaneous estimates to 6-month evolutions. As far as volcanic sulfates are concerned, these aerosols usually scatter sunlight back to space, cooling the Earth's surface, and absorb outgoing thermal radiation. Several authors have made the hypothesis that HTHH eruption could impact climate not through surface cooling due to sulfate aerosols, but rather through surface warming due to the radiative forcing from the excess stratospheric water vapor. The impact on the Earth's radiation budget, i.e. at the top of the atmosphere, is even more uncertain since smaller impacts, hence a greater sensitivity to variations, are at play. To date, assessments of the radiative effect of combined water vapor and aerosols have only been performed for 3 case studies during the first 10 days after the eruption by (Sellitto et al., 2022) and for the first two months after the eruption by (Zhu et al., 2022).

Here, the impact of water vapor and aerosols on the Earth's radiation budget is estimated over Reunion Island (21°S, 55°E) for the first thirteen months after HTHH eruption. Both water vapor and aerosols are fully parametrized in a state-of-the-art radiative transfer model by means of ground-based lidar and satellite measurements. The radiative effect is calculated for three scenarios considering aerosols only, water vapor only and combined aerosols and water vapor.

2 Materials and Methods

2.1 The Maïdo instrumentation

Two lidar systems located at the Observatoire de Physique de l'Atmosphère à La Réunion (OPAR) Maïdo station (21.079°S, 55.383°E, 2160m asl; Baray et al., 2013) are used in this study: the Li1200 lidar operating at 355 nm with 87 nights of observations between 19 January 2022 and 15 February 2023 and the LiO3T lidar operating at 532 nm with 55 coincident nights (19 January

2022 to 13 September 2022). Details on these systems can be found in (Baron et al., 2023) and references therein.

The extinction coefficients presented in this work are obtained applying the elastic, 2-component inversion algorithm (Klett, 1985) using a constant lidar ratio (LR). Several LR values were tested between 40 and 70 sr at both wavelengths. The value of 60 sr was fixed for this study: it is the value that gives the best agreement between OMPS and lidar sAOD after complete, homogenous global dilution of the plume in the last 10 months of our dataset (see Section 3). The transmittance method initially used in (Baron et al., 2023) for the thick plume observed during the first days after the eruption over Reunion Island was not retained for at least two reasons: with decreasing aerosol loads, the transmittance method would have led to large uncertainties in the LR retrieval; the unreliability of the method for ground-based systems in low aerosol loads and at such altitude levels (17 – 32 km). However, both Klett and transmittance methods were compared for significant aerosol loads (i.e. in the first three months after the eruption) and a good agreement was obtained for the value of 60 sr. Note that this value is also in the range of what is expected for sulfate aerosols in the available literature (Lopes et al., 2019). During the first 55 measurements for which coincident 355- and 532-nm sAOD are available, namely between 19 January until 13 September, the Ångström exponent calculated between the lidar-derived sAOD at 355 and 532 nm, $AE_{355/532}$, was computed. For the rest of the measurements at 355 nm, i.e. after 13 September 2022, $AE_{355/532}$ was set to the value of 1.5 calculated for the stabilized period 13 June 2022 – 13 September 2022 (see Section 3). The uncertainty associated to the extinction profiles at 355 nm, and by extension to the sAOD at 355 nm, has been calculated considering an uncertainty on the lidar ratio of ± 10 sr. This uncertainty of ± 10 sr on the lidar ratio is the largest uncertainty calculated at 355 nm by (Baron et al., 2023) for the HTHH plume over Reunion Island in January 2022. The uncertainty associated to the sAOD at 745 nm has been calculated considering both the uncertainty associated to sAOD at 355 nm and the uncertainty associated to $AE_{355/532}$, fixed to a constant value of ± 1.0 (Baron et al., 2023).

It is our belief that the results in Reunion Island can be easily generalized throughout the southern tropical Indian Ocean region. (Mallet et al., 2018) reported for the first time the pristine characteristics of the southern Indian Ocean region located between 10 and 40°S and between 50 and 110°E. Except its very northern boundary, this domain is not impacted by the longitudinal transport of the Asian monsoon over the northern Indian Ocean. Tropospheric sea salt aerosols are the dominant and the AOD-modulating aerosol type (Mallet et al., 2018). The same statement is true over Reunion Island (Duflot et al., 2022). The synoptic circulation in the southern tropical Indian Ocean is strongly connected with the Mascarene anticyclone, which, because of its location in the middle of this basin, limits the transport of terrestrial aerosols to this region. Several indicators of the homogenous dilution of the volcanic plume in the stratosphere are exposed in Section 3 and reinforce the assumption made from now that the results in Reunion Island can be generalized to the whole southern tropical Indian Ocean region.

2.2 Satellite and reanalysis data

The Ozone Mapper and Profiler Suite (OMPS) Limb profiler has been on-board the Suomi National Polar Partnership (NPP) since October 2011. Using limb scattering solar radiation, OMPS provides good quality of aerosols extinction retrievals at several wavelengths: 510, 600, 675, 745, 869 and 997 mm (Taha et al., 2021). As recommended by the latter, we use data product version 2.0 of aerosol extinction profile at 745 nm to follow the aerosol volcanic plume over Reunion Island, from January 2022 to mid-April 2023. These data are provided from 10 to 40 km height on

a vertical grid of 1 km. Stratospheric aerosol optical depth calculations are made by integrating the extinction profiles from 17 km to 40 km, where 17 km corresponds to tropopause height over Reunion Island (Bègue et al., 2010). Based on previous studies in the Southern Hemisphere (Bègue et al., 2017; Tidiga et al., 2022), background periods extend from 2012 to February 2014 and from January 2017 to April 2018, to exclude volcanic eruptions (Kelud, Calbuco, Ambae and Ulawun) and Australian 2019/2020 biomass burning episode (the Black Summer).

The MERRA-2 Stratospheric Composition Reanalysis of Aura MLS (M2-SCREAM) products are used for characterizing the water vapor (WV) and ozone vertical distribution, in particular the 3D, 3-hourly GMAO_M2SCREAM_INST3_CHEM product available until 1 April 2023 (doi: 10.5067/7PR3XRD6Q3NQ). This product, produced at NASA's Global Modeling and Assimilation Office (GMAO), is generated by assimilating MLS (Microwave Limb Sounder) and OMI (Ozone Monitoring Instrument) retrievals into the GEOS (Goddard Earth Observing System) Constituent Data Assimilation System (CoDAS) driven by meteorological fields from MERRA-2. Stratospheric water vapor and ozone, among other compounds, are assimilated in M2-SCREAM. Assimilated fields are provided globally at 0.5° (latitude) by 0.625° (longitude) resolution from approximately 10 km up to the lower thermosphere. Concretely, the variables of specific humidity (QV, kg kg^{-1}), ozone (O3, ppmv), mid-layer pressure (PL, Pa) and mid-layer height (H, m) were used. The specific humidity was converted to the actual water vapor pressure and then to water vapor mixing ratio. All variables where averaged over four pixels surrounding the Maïdo coordinates. Assimilation uncertainties for each of the assimilated constituents are calculated from the CoDAS statistical output (Wargan et al., 2023). For the period January 2022 to September 2022 and in the height interval of interest of this study (17 – 32 km) the uncertainty on the water vapor and ozone are less than 0.2 and 0.13 ppmv (Wargan et al., 2023), respectively.

MLS version 5.0, level 3 data are also used to extract the monthly mean water vapor over our site and in the stratosphere during 2021 to serve as a climatological reference. See https://mls.jpl.nasa.gov/data/v5-0_data_quality_document.pdf for more details about this MLS product. The monthly mean of the water vapor in the altitude range of interest in 2021 is 4.5 ppmv. This value sets the climatological reference necessary to parametrize the unperturbed conditions of the water vapor.

2.3 The GAME radiative transfer model: code and parametrization

Radiative fluxes propagating through the atmosphere were calculated with the radiative transfer (RT) model GAME (Dubuisson et al., 1996; Dubuisson, 2004; Dubuisson et al., 2006). For this study, GAME was set up to calculate spectrally integrated upward and downward radiative fluxes in 40 plane and homogeneous layers from 0 to 100 km with a 1 km resolution from 0 to 30 km and a coarser resolution above. The shortwave (SW) spectral range was set from 0.2 to 4.0 μm (wave number resolution of 400 cm^{-1} from 0.2 to 0.7 μm and 100 cm^{-1} from 0.7 to 4.0 μm). In the longwave (LW) spectral range, spectral limits were defined between 4.0 and 50.0 μm (115 points at a wave number resolution of 20 cm^{-1}). GAME calculates solar flux values at the boundary of plane and homogenous atmospheric layers by using the discrete ordinates method (Stamnes et al., 1988). Gas (H_2O, CO_2, O_3, N_2O, CO, CH_4, and N_2 are considered) absorption is calculated from the correlated *k* distribution (Lacis & Oinas, 1991). More details about the computation of the gas transmission functions can be found in (Dubuisson, 2004) and (Sicard et al., 2014). In the longwave spectral range, GAME presents the advantage of the complete representation of the long-wave aerosol scattering, in addition to their absorption (Sicard et al., 2014).

For the sake of clarity and comparability with other works, we recall the definition of the direct radiative effect (DRE) of a perturbed vs. unperturbed atmospheric compound on the Earth-Atmosphere radiative budget. At a given height level, L:

$$DRE(L) = \left[F_p^{\downarrow}(L) - F_p^{\uparrow}(L)\right] - \left[F_u^{\downarrow}(L) - F_u^{\uparrow}(L)\right] \quad (1)$$

where F are the radiative flux values for the perturbed (p subindex) and unperturbed (u subindex), while the ↓ and ↑ arrows indicate, respectively, the downward and upward flux direction. By that definition, negative (positive) DRE values represent a cooling (warming) effect. The DRE was calculated at two climate-relevant altitude levels: at the top of atmosphere (TOA) and at the bottom of atmosphere (BOA). The contribution in the atmospheric column is quantified by the atmospheric direct radiative effect, $DRE(ATM)$, which is defined as follows:

$$DRE(ATM) = DRE(TOA) - DRE(BOA) \quad (2)$$

As far as GAME parametrization is concerned, temperature and pressure profiles used in both SW LW simulations are taken from radiosoundings launched from Saint-Denis, the state capital of Reunion Island, 20 km North of Maïdo, every night at 00:00 Local Time. Aerosols are fully parameterized in GAME by the user in terms of spectrally and vertically resolved aerosol optical depth (AOD), single scattering albedo (SSA), and asymmetry factor (asyF).

In the SW spectral range, the spectral sAOD was calculated with the lidar extinction coefficients at 355 nm and $AE_{355/532}$. Spectral SSA and asyF were interpolated from the four-wavelength AERONET L1.5 monthly means and assumed constant above 1020 nm. The spectral surface albedo was interpolated from the four-wavelength AERONET L2.0 annual (2022) mean and assumed constant above 1020 nm.

In the LW spectral range, a Mie code was used to calculate the LW spectral AOD, SSA and asyF. The bimodal, lognormal size distribution was considered. Geometric median radii and standard deviations were calculated from AERONET L1.5 fine and coarse mode volume median radii and standard deviations applying Eq. (A2) and (A3) of (Sicard et al., 2014). For the refractive index we used the GEISA (Gestion et Étude des Informations Spectroscopiques Atmosphériques: Management and Study of Spectroscopic Information) spectroscopic database (Jacquinet-Husson et al., 2008). In particular the refractive index of the binary system H_2SO_4/H_2O with a H_2SO_4 mixing ratios (in mass, i.e., the ratio of the H_2SO_4 mass to the total mass of the droplets) of 75 % and at temperature of 215 K (this temperature corresponds in average to the atmospheric temperature at the height of the volcanic plume) was used. For comparison, (Bernath et al., 2023), who analyzed measurements of atmospheric infrared transmittance of the HTHH sulfate aerosol plume by the Atmospheric Chemistry Experiment satellite 20 days after the eruption, found a H_2SO_4 mixing ratio of 62.5 %. The real part is defined over the range 0.61 – 5000.00 µm (wave number resolution of 2 cm^{-1}), while the imaginary part is defined over the range 2.36 – 23.15 µm (wave number resolution of 0.96 cm^{-1}). The reader is referred to (Biermann et al., 2000) for more details on this dataset. Figure 1 shows the real part (RRI) and imaginary part (IRI) of the refractive index used. Large spectral variations in the infrared atmospheric window (8–13 µm), which have an important impact on the infrared radiative budget of the atmosphere, are visible. The most astonishing feature of the figure is probably the high absolute values of the IRI which emphasizes the high absorbing properties of sulfate aerosols in the longwave spectral range. For comparison IRI (this study) is 2 to 3 times larger in the atmospheric window than IRI for mineral dust (Sicard et al., 2014). Finally, for the LW broadband surface albedo, we used IASI (Infrared Atmospheric

Sounding Interferometer) December nighttime monthly mean climatology of the surface emissivity (i.e. 1 - surface albedo) at 890 cm^{-1}, i.e. 11.24 µm, over the Indian Ocean (Zhou et al., 2013), and set the surface albedo value to 0.01.

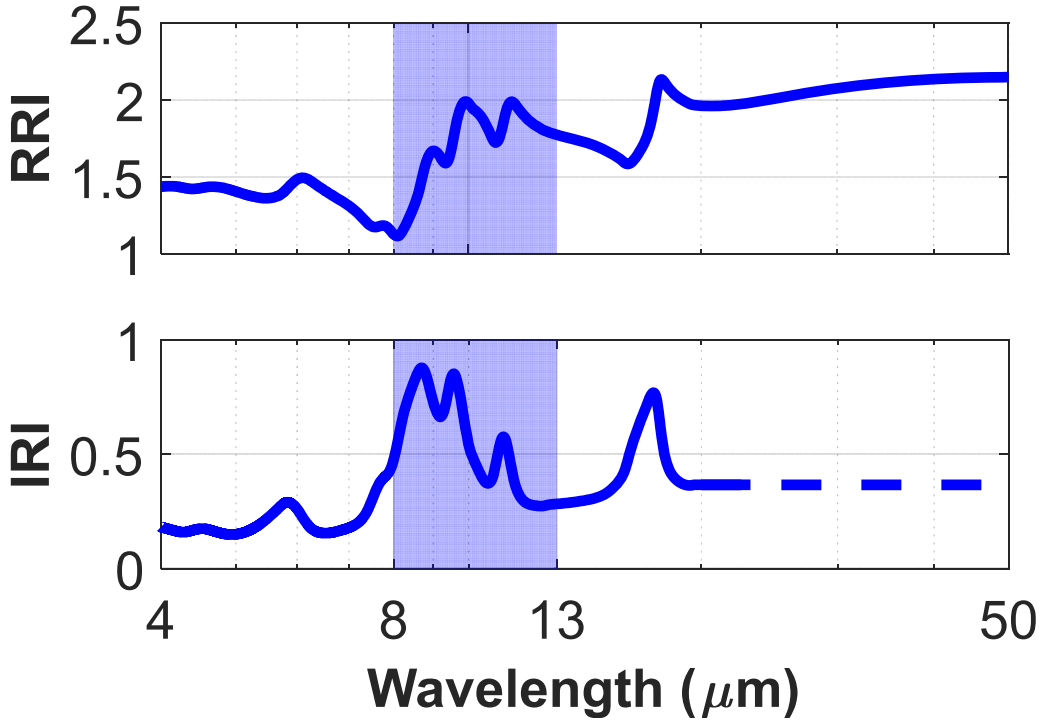

Figure 1. Spectral complex refractive index considered for the calculation of the aerosol radiative properties in the longwave spectral range. See text for details. The infrared atmospheric window (8–13 µm) is indicated by the blue shaded area. The dash line in IRI is the extrapolation of the dataset used up to 50 µm.

So as to avoid the dependency on solar zenith angle, only daily radiative effects are presented in this work. To do so, each nighttime measurement and parametrization is assumed to be constant for the 24 hours of the day considered and both SW and LW radiative effects are calculated at an hourly time resolution between 00:00 and 23:00 UT. In these calculations, the solar zenith angle is the only parameter that varies. The daily radiative effect is the average of the 24 hourly DRE.

3 Vertical/temporal evolution of the HTHH volcanic plume over Reunion Island

The historical context of the aerosol load over Reunion Island is shown by the temporal evolution of the stratospheric AOD at 745 nm measured by OMPS in the last decade (Figure 2). The background sAOD is measured over the unperturbed years 2012 and 2013. It is $(2.59 \pm 0.10) \times 10^{-3}$. At each exceptional event the sAOD takes off from this background sAOD and since the eruption of Ambae in July 2018 the sAOD over Reunion Island has never turned back to its background value. The sAOD peak produced by HTHH (0.035) is the highest in the last decade and it is a factor 4 times higher than the second highest event (0.009, Calbuco eruption in April 2015). Zonal averages between 30ºS and 15ºN for HTHH and 20ºS and 90ºS for Calbuco showed that HTHH sAOD was more than double that for the 2015 Calbuco eruption (Taha et al., 2022). The reason why the local and zonal sAOD differences between HTHH and Calbuco differ lies in the zonal mean stratospheric conditions. In the case of HTHH, a marked easterly band (Khaykin et al., 2022;

Legras et al., 2022) favored a direct transport from HTHH towards Reunion Island (both being approximately at the same latitude). Further back historically, the 40+ year satellite record of monthly sAOD for the 60ºS – 60ºN latitude band in (Khaykin et al., 2022) shows that only the eruptions of Pinatubo (1991) and El Chichón (1982) exceeded the HTHH one in terms of absolute stratospheric AOD (by a factor of 6 and 3, respectively).

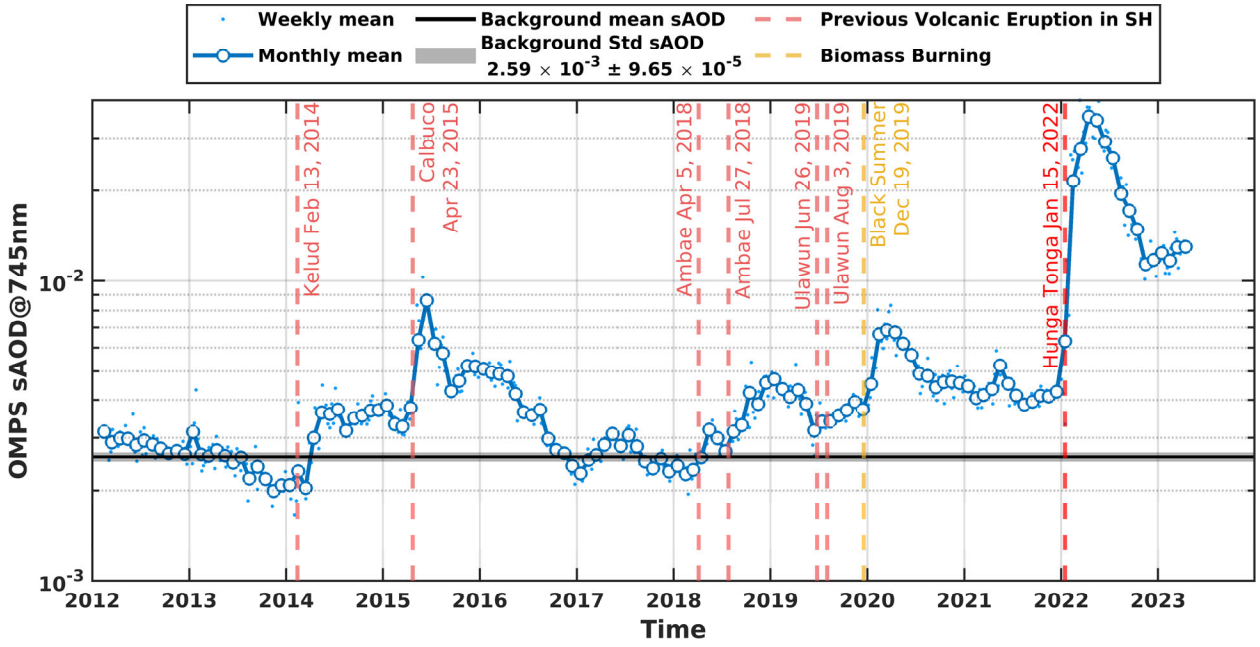

Figure 2. sAOD (17 – 40 km) at 745 nm from OMPS over Reunion Island. The most important volcanic eruptions (name and date) in the southern hemisphere are indicated by red vertical lines. The Australian 2019/2020 biomass burning episode is indicated in orange.

The vertical and temporal (January 2022 – April 2023) evolution of the HTHH volcanic plume over Reunion Island is analyzed by means of sAOD at 745 nm and profiles of extinction coefficient at 745 nm, water vapor and ozone (Figure 3). While the monthly OMPS sAOD peak is reached in April and May 2022, the instantaneous lidar sAOD peaks just a few days after the eruption, reaching 0.54 on 21 January. This time difference is an indication of the dilution time of the volcanic matter injected by HTHH in the stratosphere at the global scale. Other studies confirm that the volcanic plume dispersed nearly pole-to-pole in three months (Khaykin et al., 2022; Taha et al., 2022). Another indicator of this dilution is the standard deviation (calculated as a 15-day rolling standard deviation) associated to OMPS monthly sAOD: once passed the first month, it steadily decreases all along year 2022. The agreement between monthly and instantaneous sAOD which becomes excellent as of September 2022 is also an indicator of the homogenous dilution of the volcanic plume in the stratosphere. It also reinforces our belief that these results in Reunion Island could probably be generalized throughout the southern tropical Indian Ocean region. A decrease of the monthly sAOD is observed after April/May and until November. Then sAOD stabilizes until today (sAOD = 0.012, almost 5 times the background sAOD). The Ångström exponent calculated between the lidar-derived sAOD at 355 and 532 nm, $AE_{355/532}$, has near-zero values during the first two weeks after the eruption (Baron et al., 2023), indicating a probable mixing of fine-mode sulfate and coarse-mode non-sulfate (ash/ice particles) aerosols as suggested by (Sellitto et al., 2022). After one month (not shown) $AE_{355/532}$ reaches values above 1.3 that stabilize rapidly at 1.5.

The time-height plot of the extinction coefficient (Figure 3b) shows clearly the height and vertical extension of the volcanic plume which is still present on 15 April 2023 and located at 18.5 – 23.5 km height (sAOD = 0.012). The plume peak height has a decreasing tendency since April 2022 at an average steady rate of -244 m per month or ~ -0.008 km day^{-1}. Assuming this rate constant in time and a tropopause height in Reunion Island of 17 km (Bègue et al., 2010), the remaining life time of the volcanic plume in the stratosphere is estimated to be between 2 and 2.5 years after 15 April 2023. Except during the first week of detection above Reunion Island, the HTHH volcanic plume is not detected above 30 km. The water vapor plume (Figure 3c) reveals also clearly the unusually high water vapor concentration caused by the volcanic plume. A local peak of 65 ppmv is reached on 13 February 2022. It is almost 15 times higher than the climatological reference value of 4.5 ppmv (see Section 2.2). On a monthly basis, the water vapor stratospheric peak in February 2022 is approximately 5 times higher than the climatological reference (4.5 ppmv). This ratio decreases to almost 2 in February 2023. The water vapor plume is thinner than the aerosol one and located at a higher altitude, 3 to 4 km higher. Such a difference is observed at the zonal

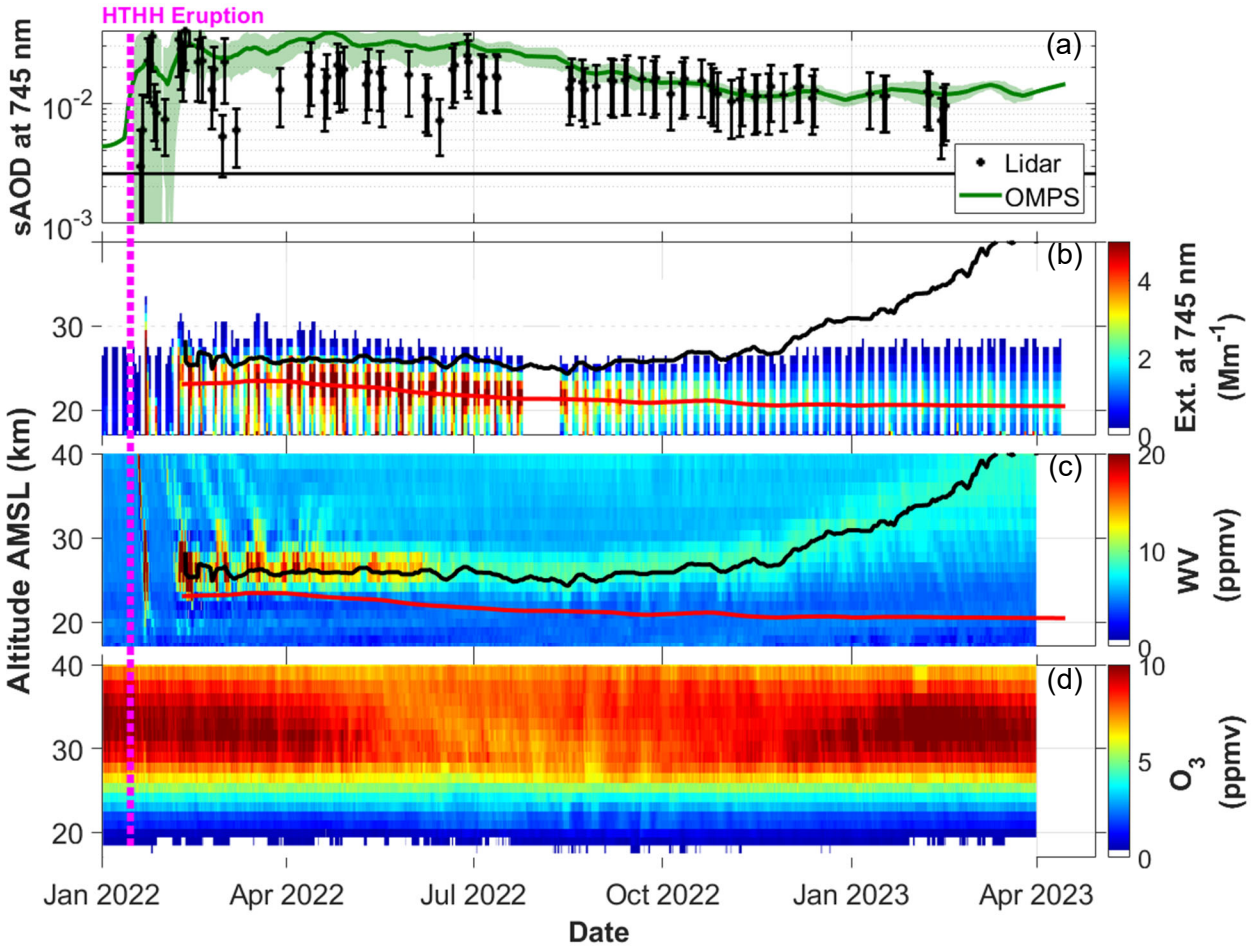

Figure 3. (a) Monthly (OMPS) and instantaneous (lidar, nighttime) sAOD (17 – 40 km) at 745 nm over Reunion Island; Time-height plots of (b) extinction coefficient at 745 nm from OMPS, (c) water vapor and (d) ozone mixing ratio from M2-SCREAM. The red and black lines in (b) and (c) report the peak height of the aerosol and water vapor plumes, respectively.

scale (at 15º S), although not so accentuated, during the first six months of year 2022 (Schoeberl et al., 2022). The height of the peak of the aerosol and water vapor layers (respectively, red and black lines in Figure 3b and Figure 3c) have opposite tendencies as of April 2022: the aerosol plume is slowly descending whereas the moist layer is ascending slowly until October 2022 and at a higher rate afterwards. (Schoeberl et al., 2022) explain that "the water vapor is transported upward with the diabatic circulation that gives rise to the tropical trace gas tape recorders (Schoeberl et al., 2018) whereas the aerosols are gravitationally settling". (Legras et al., 2022) who analyze the same period (first six months of year 2022) precise that the ascent of the moist layer is due to the Brewer–Dobson circulation. The ozone cycle (Figure 3d) with highs in the austral summer (January-April) and lows in the austral winter (July-October) reflects the higher production of ozone in summer due to the peak of solar radiation compared to winter (Abdoulwahab, 2016). Apart from this natural cycle of stratospheric ozone at subtropical latitudes, no other spatio-temporal variation, potentially caused by HTHH eruption, is visible at naked eye in Figure 3d. Some authors mention that, following HTHH eruption, ozone concentrations increase in the middle stratosphere and decrease in the lower stratosphere were caused by enhanced sulfate aerosol (Lu et al., 2023), others claimed that the midlatitude and tropics ozone reduction observed by MLS was mainly linked to circulation effects (Wang et al., 2022). At this early stage of our understanding of the effects of HTHH on the stratospheric ozone, the present study does not consider any potential increase/decrease of stratospheric ozone due to HTHH eruption.

4 Impact of the HTHH volcanic plume on the Earth's radiation budget

In order to analyze the radiative impact of the aerosols and the water vapor, separately and altogether, 4 runs of GAME are performed and summarized in Table 1. The perturbed condition is the full parametrization with observed sAOD and water vapor mixing ratio. For the unperturbed conditions, the impact of aerosols is assessed by assuming an aerosol-free stratosphere; the impact of water vapor is assessed by assuming that the water vapor mixing ratio in the HTHH moist layer is equal to the climatological value of 4.5 ppmv obtained from the MLS 2021 monthly means; the impact of aerosols and water vapor is assessed by assuming both an aerosol-free stratosphere and a water vapor mixing ratio of 4.5 ppmv in the HTHH moist layer.

Impact of…	Perturbed	Unperturbed
Aerosols	Measured sAOD Measured WV	sAOD = 0 Measured WV
Water vapor		Measured sAOD WV = 4.5 ppmv above 20 km (climatology from MLS monthly means in 2021)
Aerosol and water vapor		sAOD = 0 WV = 4.5 ppmv above 20 km (climatology from MLS monthly means in 2021)

Table 1. Aerosol and water vapor parametrization for the perturbed/unperturbed simulations of GAME.

Figure 4, Figure 5 and Figure 6 show the radiative impact of aerosols only, of the water vapor only, and of both aerosols and water vapor, respectively, in terms of time plots of $DRE(BOA)$ and $DRE(TOA)$ as well as time-height plots of heating/cooling (H/C) rate anomaly in the SW, LW and SW+LW spectral ranges.

In the first four months after the eruption, the aerosol LW dominates over the SW component at TOA (Figure 4a), producing a net warming (positive) radiative effect. After May 2022, both components roughly compensate: $|DRE(TOA)| < 0.6$ W m^{-2}. Interestingly, during the first week $DRE(TOA)$ is negative. It presents a peak at -13.8 W m^{-2} which falls in the range of instantaneous values found by (Sellitto et al., 2022) for the fresh plume (-19.4 and -12.1 W m^{-2}). This change of sign is attributed to a combination of facts: the high sAOD measured over Reunion Island during the first week after the eruption (Baron et al., 2023) and smaller SW asymmetry factors for the month of January 2022 (implying an increase of the solar radiation reflected back to space). We also observed a smaller fine mode radius in January 2022 compared to the rest of the period, also evidenced by (Boichu et al., 2023) over Reunion Island, but this is not expected to affect significantly the LW radiative properties (Sicard et al., 2014). (Zhu et al., 2022) who use a global climate model to simulate the radiative effect in the first two months of 2022 find that when only volcanic sulfur dioxide is present (without water vapor) the zonal $DRE(TOA)$ at the latitude of Reunion Island is negative. This is opposite of our results, but somehow expected since their model underestimates the production of sulfate particles (i.e., it underestimates sAOD) when water injection is not considered. At BOA the aerosol LW component is nearly zero, so that the aerosol net DRE is that of the SW component: a cooling is observed. A peak is observed during the first week after the eruption at -26.8 W m^{-2} and again it falls in the range of instantaneous values found by (Sellitto et al., 2022) for the fresh plume (-27.9 and -17.5 W m^{-2}). As a consequence of $DRE(TOA)$ and $DRE(BOA)$, and as illustrated by the time-height plots of H/C rates (Figure 4d), the atmosphere warms, mostly because of the aerosol LW warming. The SW+LW aerosol impact in the stratosphere is mostly positive with daily heating rates of ~ +1.00 ºK day^{-1} in the first 4-6 months, and ~ +0.06 – +0.15 ºK day^{-1} afterwards. The H/C rate profiles follow the shape of the aerosol extinction profiles with a decreasing tendency starting in April 2022 (Figure 3b). In conclusion, the effect caused by aerosols only is what is usually expected for stratospheric sulfate aerosols (Bernath et al., 2023): HTHH stratospheric particles measured over Reunion Island scatter sunlight back to space, cooling the Earth's surface and absorb outgoing longwave radiation, heating the stratosphere.

The water vapor radiative effect (Figure 5) is dominated by the cooling effect of water vapor longwave emission in the moist layer. This layer produces a slightly negative effect at TOA ($|DRE(TOA)| < 0.3$ W m^{-2}) and a neutral effect (~ 0 W m^{-2}) at BOA. (Sellitto et al., 2022) estimated also a negative $DRE(TOA)$ caused by water vapor for the fresh plume (instantaneous values of -0.7 and -0.4 W m^{-2}), but a positive $DRE(TOA)$ caused by water vapor for the aged plume (8 February 2022) of +0.8 W m^{-2} and attributed to the descent in altitude of the moist layer. Our analysis does not support this change of sign. (Zhu et al., 2022) find that when only water vapor is injected in their model (without sulfur dioxide; see their supplementary material) the zonal $DRE(TOA)$ at the latitude of Reunion Island is positive and much smaller than that caused by aerosols. The discrepancy with our findings stems from an excess of water vapor in (Zhu et al., 2022) simulations since the reaction of sulfur dioxide (not present) and hydroxide is not happening in their simulation; different heights of the moist layer; and/or zonal vs. local computations. The SW+LW water vapor radiative impact in the stratosphere is mostly negative with daily cooling

rates of ~ -0.20 – -0.40 ºK day^{-1} in the first 4-6 months, and ~ -0.06 – -0.15 ºK day^{-1} afterwards. The same ascending behavior of the water vapor concentration (Figure 3c) is observed on the profiles of the LW water vapor cooling rate (Figure 5c). (Schoeberl et al., 2022), who estimated the LW zonal impact of water vapor at 15º South for the first 6 months of year 2022, show a cooling effect in the stratosphere with a peak at ~ -0.5 ºK day^{-1} at the end of February and decreasing afterwards. (Sellitto et al., 2022) calculated instantaneous cooling rates peaking between -4.0 and -10 ºK day^{-1}.

When aerosols and water vapor HTHH perturbations are considered together (Figure 6), the radiative effect both at TOA and BOA is similar to that of the aerosols only (Figure 4): positive at TOA until April 2022 and switching to negative-to-neutral afterwards, and negative at BOA. These effects (warming/cooling/neutral) are in agreement with the estimations made by (Sellitto et al., 2022) for what they call the "aged plume". In a third simulation performed by (Zhu et al., 2022) where both sulfur dioxide and water vapor are injected, these authors find a negative radiative effect at both TOA and BOA which, averaged globally and limited to the first 2 months of 2022, are equal to -0.21 and -0.21 W m^{-2}, respectively. The discrepancy with our results at TOA seems to speak against the different methodologies used, and in particular to the amount of volcanic aerosols used in both works: a function of the water vapor injected (Zhu et al., 2022) and measured by lidar (this study). Our results imply that the missing energy at the surface is trapped in the stratospheric volcanic layer which warms: the total atmospheric radiative budget is positive and generally exceeds +1.0 W m^{-2} in the first 4-6 months after the eruption and is on the order of +0.4 – +1.0 Wm^{-2} afterwards, the causing agent being the positive aerosol LW $DRE(ATM)$ (nearly 10 times larger than the WV component of opposite sign) reflecting the strong aerosol LW warming w.r.t. a moderate water vapor LW cooling.

An interesting result at this point is how the aerosols and water vapor H/C rates distribute vertically in the atmosphere. It is clear from Figure 6d that the longwave cooling caused by water vapor and warming caused by the aerosols coexist at different altitude levels. To further discuss this issue, we analyze three different periods of time, excluding from now on the first two weeks after the eruption to allow for some dilution to happen:

- The entire period from Feb. 2022 to Feb. 2023 (M2 – M13, M1 being Jan. 2022).
- Feb. 2022 – Apr. 2022 (M2 – M4), short-term period: aerosol and WV $DRE(TOA)$ is positive.
- May 2022 – Feb. 2023 (M5 – M13), mid-term period: aerosol and WV $DRE(TOA)$ is negative-to-neutral.

The first period is representative of the radiative impact of HTHH since the eruption to date, while the second and third periods are representative of the short- and mid-term tendencies, respectively. Figure 7 shows the averaged H/C rate anomaly profiles over the three periods for the last simulation performed (aerosols and water vapor). The radiative effects of the three simulations (aerosols only, WV only, aerosols and WV) associated to the three periods at the three atmospheric level (BOA, ATM, TOA) are summarized in Table 2. Independently of the period considered, the WV cooling peak, related to unusually high WV concentration at that altitude in the first 4-6 months after the eruption (see Figure 3c), occurs at 27 km. The aerosol positive peak occurs at 25 km during M2 – M4 and drops to 22 km during M5 – M13. The change of sign of the profiles occurs at 26 km for the entire period, while it is a little higher (~26-27 km) during M2 – M4 and lower (~24-25 km) during M5 – M13, in agreement with the descent of the volcanic aerosol layer.

At the southern hemisphere scale (60ºS – 10ºS), (Wang et al., 2022) estimated a stratospheric temperature anomaly from MLS measurements at 25 hPa (~ 25 km at the latitude of Reunion Island) of ~ -1ºK on 1 November, 2022. This negative temperature anomaly seems in agreement with the sign (negative) of the heating/cooling rate profile observed at 25 km for the mid-term period M5 – M13. Interestingly, note the effect of the rapid vertical displacements of positive/negative rate anomalies (Figure 6d) in the short-term period which, once averaged, compensate at 23 and 24 km and thus result in a neutral (zero) H/C rate at these altitudes (Figure 7). In terms of shape and magnitude, the short-term period M2 – M4 exhibits marked and steep variations with positive and negative peaks of similar intensity (0.27 ºK day^{-1} in absolute value). During the mid-term period (M5 – M13) the homogeneous dilution of the plume makes the H/C rate vertical distribution much smoother with also comparable positive and negative peaks at ~0.13 ºK day^{-1} in absolute value. However, because the WV cooling occurs at higher altitudes than the aerosol warming, what drives the stratospheric radiative effect is that of the aerosols (warming): $DRE(ATM)$ = +1.79 ± 1.43 W m^{-2} for the short-term period (M2 – M4) and +0.63 ± 0.22 W m^{-2} for the mid-term period (M5 – M13). It is +0.97 ± 0.95 W m^{-2} over the first thirteen months after the eruption. We can state without any doubt that this warming effect would have been reduced to a likely neutral effect ($DRE(ATM)$ ~ 0 W m^{-2}) if aerosols and water vapor had been present at the same altitude levels.

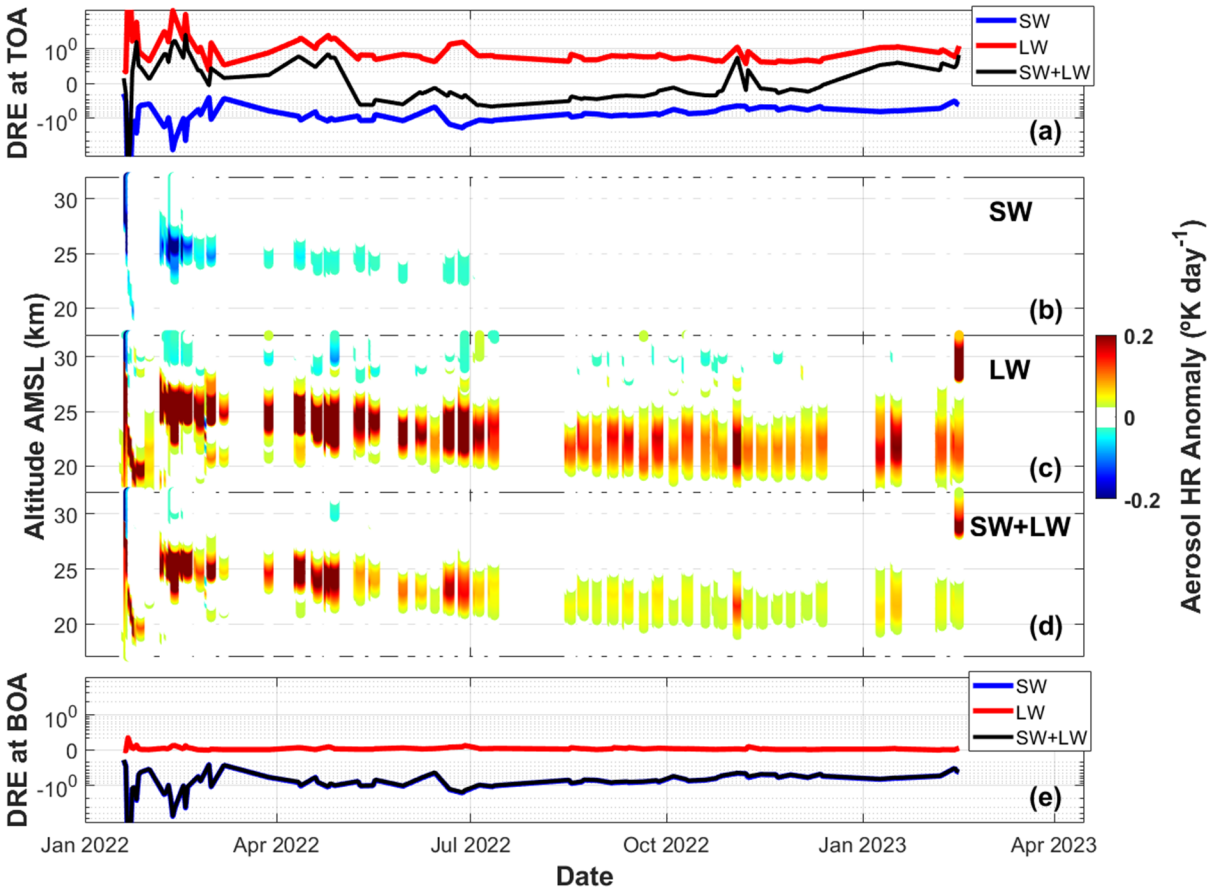

Figure 4. Aerosol direct radiative impact. (a) Radiative effect (W m^{-2}) at TOA; Time-height evolution of the H/C rate anomaly in the (b) SW; (c) LW; and (d) SW+LW spectral ranges; (e) Radiative effect (W m^{-2}) at BOA.

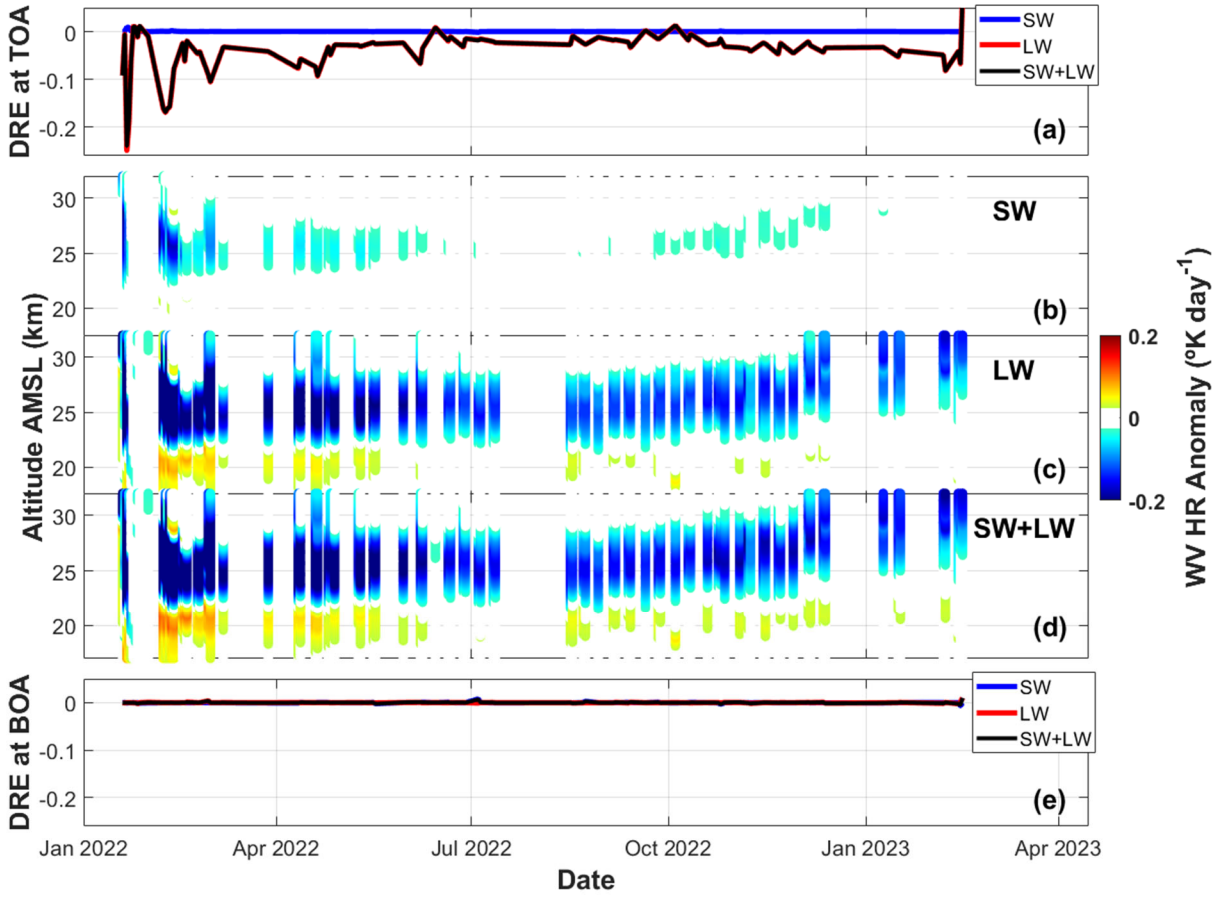

Figure 5. Idem as Figure 4 for the water vapor. Note that the left axis scale in (a) and (e) is different from that of Figure 4.

Finally, the overall HTHH aerosol and water vapor impact on the Earth's radiation budget (Table 2) is positive (warming) for the first thirteen months after the eruption: $DRE(TOA) = +0.06 \pm 0.45$ W m^{-2}. The aerosol warming dominates, so far, for this period. However, the breakdown in short- and mid-term tendencies shows that the predominance of the aerosols at TOA decreases with time: $DRE(TOA)$ is strongly positive ($+0.53 \pm 0.48$ W m^{-2}) during M2 – M4 and switches sign (-0.13 ± 0.26 W m^{-2}) during M5 – M13. Given the large standard deviations associated, these numbers should be taken with caution. Several facts and hypothesis support this evolution. By looking back to Figure 3a, one sees that, between April and November 2022, sAOD is quantitatively decreasing with time faster than the slow decaying stratospheric water vapor (Khaykin et al., 2022). In addition, the volcanic aerosol plume decreases in height while the moist layer ascends. Both effects reinforce the radiative efficiency at TOA of water vapor against volcanic aerosols, and are part of the reason why $DRE(TOA)$ changes sign from positive to negative. In the longer term, $DRE(TOA)$, averaged over the whole post-eruption period, might reduce to quasi-neutral, or even become slightly negative. At the global scale, (Zhu et al., 2022), mentioned earlier, find a $DRE(TOA)$ of -0.21 W m^{-2} for the first two months of 2022; their estimation is of opposite sign compared to this study (see two paragraphs above for explanation). At the surface, the results are more conclusive: a cooling produced by HTHH volcanic aerosols is observed ($DRE(BOA) = -0.91$

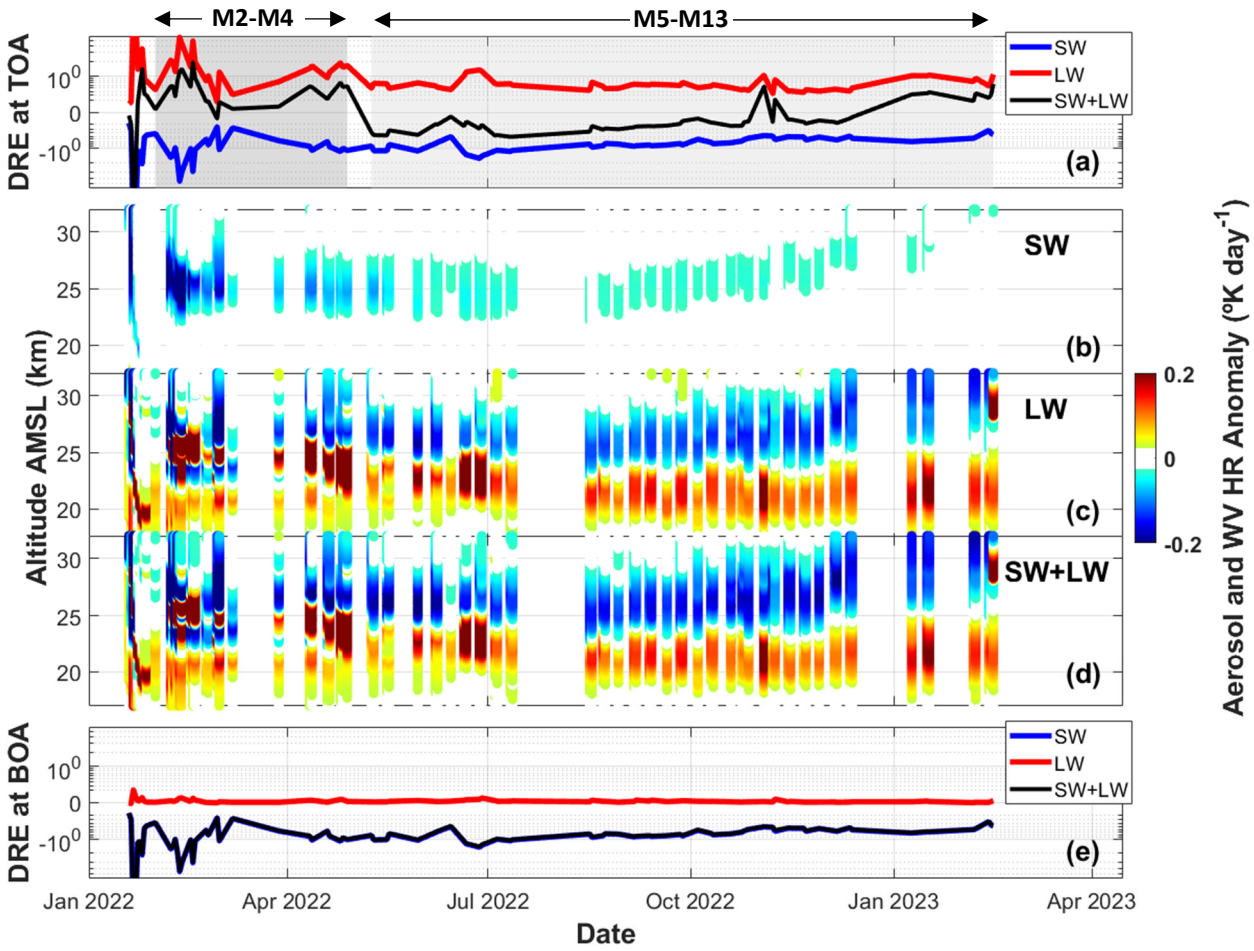

Figure 6. Idem as Figure 4 for the aerosols and water vapor. In (a), the gray shaded areas represent the short- and mid-term periods: February to April 2022 (M2 – M4) and May 2022 to February 2023 (M5 – M13).

± 0.61 W m^{-2} for the entire period), with a decreasing tendency with time ($DRE(BOA)$ = -1.26 ± 0.99 W m^{-2} for M2 – M4 and -0.76 ± 0.23 W m^{-2} for M5 – M13). (Zuo et al., 2022) modeled the global surface temperature in the first year after the HTHH eruption and found a negative anomaly of -0.004 ºK but recognized that it is "within the amplitude of internal variability at the interannual time scale and thus not strong enough to have significant impacts on the global climate". In contrast, by extension of our results to the southern tropical Indian Ocean region, our analysis shows that the eruption of HTHH might have had a clear cooling impact on the regional climate at the surface in this region of the Earth.

5 Conclusions

Thirteen months after the eruption of HTHH volcano, aerosols and water vapor are still present in the stratosphere of the southern tropical Indian Ocean region. During the first three months after the eruption the stratospheric aerosol optical depth increases and reaches a peak at 0.035 (~13 times the background sAOD) in April 2022, the highest in the last decade, and the third highest in the last 40 years (after Pinatubo and El Chichón). From April to November 2022 the sAOD decreases and then stabilizes at a value of 0.012 (~5 times the background sAOD). Unusually high water vapor concentrations are also observed in the stratosphere. On a monthly basis, the water

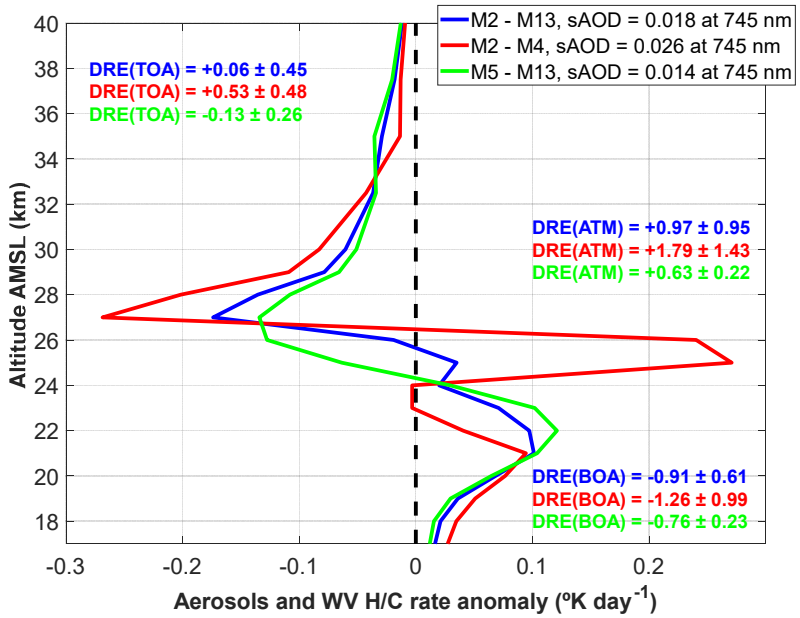

Figure 7. Profiles of aerosol and water vapor daily heating/cooling rate anomaly averaged over the entire period (M2 – M13), the short-term period (M2 – M4) and the mid-term period (M5 – M13), all excluding week 1 and 2 after the eruption.

	Aerosols	Water vapor	Aerosols and water vapor
Daily *DRE* (W m^{-2}) for the entire period M2 - M13			
TOA	+0.10 ± 0.47	-0.04 ± 0.04	+0.06 ± 0.45
ATM	+1.01 ± 0.97	-0.04 ± 0.04	+0.97 ± 0.95
BOA	-0.90 ± 0.61	< 0.01	-0.91 ± 0.61
Daily *DRE* (W m^{-2}) for the short-term period M2 – M4			
TOA	+0.60 ± 0.49	-0.07 ± 0.05	+0.53 ± 0.48
ATM	+1.86 ± 1.44	-0.07 ± 0.05	+1.79 ± 1.43
BOA	-1.26 ± 0.99	< 0.01	-1.26 ± 0.99
Daily *DRE* (W m^{-2}) for the mid-term period M5 – M13			
TOA	-0.11 ± 0.27	-0.03 ± 0.02	-0.13 ± 0.26
ATM	+0.65 ± 0.22	-0.03 ± 0.02	+0.63 ± 0.22
BOA	-0.76 ± 0.23	< 0.01	-0.76 ± 0.23

Table 2. SW+LW *DRE* at BOA, TOA and in the atmosphere produced by aerosols only, WV only and both aerosols and WV. These values are the average over the entire period M2 – M13, the short-term period M2 – M4, and the mid-term period M5 – M13, all excluding week 1 and 2 after the eruption.

vapor stratospheric peak reaches a maximum in February 2022 which is approximately a factor 5 above the climatological reference. In February 2023, this ratio has decreased down to almost 2.

In all moments, the water vapor plume is located at a higher altitude than the aerosol plume. The height of the peak of the aerosol and water vapor layers have opposite tendencies as of April 2022: the aerosol plume is slowly descending by gravitational settling whereas the moist layer is ascending slowly until October 2022 and at a higher rate afterwards. The upward transport of the moist layer is due to the Brewer-Dobson circulation. Both aerosol and WV plumes are still present on 15 April 2023. The aerosol plume is located at 18.5 – 23.5 km height and the moist layer is above 30 km. As far as aerosols are concerned, the plume peak height decreases since April 2022 at an average steady rate of ~ -0.008 km day^{-1}. Assuming this rate constant in time, the remaining life time of the volcanic plume in the stratosphere is estimated to be between 2 and 2.5 years after 15 April 2023.

The radiative impact of both aerosol and water vapor layers is estimated at our site and assumed representative of the southern tropical Indian Ocean. Averages are made over 3 different periods of time in order to explain the temporal evolution: the first thirteen months, the short-term (M2 – M4) and the mid-term (M5 – M13) periods. During the first thirteen months after HTHH eruption, the overall aerosol and water vapor impact on the Earth's radiation budget is positive (warming, $+0.06 \pm 0.45$ W m^{-2}) and dominated by the aerosol impact. However, the decreasing rate with time of the aerosol warming effect is larger than that of the water vapor cooling effect, so that, in the long run, the impact on the Earth's radiation budget might reduce to quasi-neutral, or even become slightly negative. At least two factors are at play here: between April and November 2022, sAOD is quantitatively decreasing with time faster than the slow decaying stratospheric water vapor; the volcanic aerosol plume decreases in height while the moist layer ascends. Both effects reinforce the radiative efficiency at TOA of water vapor against volcanic aerosols. At the Earth's surface, aerosols are the main driver and produce a negative (cooling, -0.91 ± 0.61 W m^{-2}) radiative impact with also a decreasing tendency with time. Heating/cooling rate profiles show a clear vertical difference in the stratosphere between the aerosol warming impact (17 to 25 km) and the water vapor cooling one (25 to 40 km). Although the aerosol warming and the WV cooling rates are not drastically different in intensity, because the first one occurs at lower altitudes than the second one, what in the end drives the stratospheric radiative effect is that of the aerosols. During the first thirteen months after HTHH eruption, aerosols and water vapor produce a warming of the stratosphere ($+097 \pm 0.95$ W m^{-2}) with also a decreasing tendency with time. This study shows that the eruption of HTHH has had, so far, a clear impact on the regional climate of the Earth-Atmosphere system in the southern tropical Indian Ocean region.

Acknowledgments

The authors from LACy acknowledge the support of the European Commission through the REALISTIC project (GA 101086690).

Open Research

The lidar data and the parametrization data used in the three simulations of the radiative transfer model will be available by the time of publication. These data will receive a doi from the library of Université de la Réunion that will be cited in the paper and listed in the Reference section.

References

Abdoulwahab, M. T. (2016). Étude de la variabilité et la tendance de l'ozone stratosphérique au-dessus des tropiques et subtropiques sud.

Asher, E., Todt, M., Rosenlof, K. H., Thornberry, T. D., Gao, R.-S., Taha, G., et al. (2022). The unprecedented rapid aerosol formation from the Hunga Tonga -Hunga Haʿapai eruption. In *AGU Fall Meeting Abstracts* (Vol. 2022, pp. A42I-01).

Baray, J.-L., Courcoux, Y., Keckhut, P., Portafaix, T., Tulet, P., Cammas, J.-P., et al. (2013). Maïdo observatory: a new high-altitude station facility at Reunion Island (21° S, 55° E) for long-term atmospheric remote sensing and in situ measurements. *Atmospheric Measurement Techniques*, *6*(10), 2865–2877. https://doi.org/10.5194/amt-6-2865-2013

Baron, A., Chazette, P., Khaykin, S., Payen, G., Marquestaut, N., Bègue, N., & Duflot, V. (2023). Early Evolution of the Stratospheric Aerosol Plume Following the 2022 Hunga Tonga-Hunga Ha'apai Eruption: Lidar Observations From Reunion (21°S, 55°E). *Geophysical Research Letters*, *50*(10), e2022GL101751. https://doi.org/10.1029/2022GL101751

Bègue, N., Bencherif, H., Sivakumar, V., Kirgis, G., Mze, N., & Leclair De Bellevue, J. (2010). Temperature variability and trends in the UT-LS over a subtropical site: Reunion (20.8° S, 55.5° E). *Atmospheric Chemistry and Physics*, *10*(17), 8563–8574. https://doi.org/10.5194/acp-10-8563-2010

Bègue, Nelson, Vignelles, D., Berthet, G., Portafaix, T., Payen, G., Jégou, F., et al. (2017). Long-range transport of stratospheric aerosols in the Southern Hemisphere following the 2015

Calbuco eruption. *Atmospheric Chemistry and Physics*, *17*(24), 15019–15036. https://doi.org/10.5194/acp-17-15019-2017

Bernath, P., Boone, C., Pastorek, A., Cameron, D., & Lecours, M. (2023). Satellite characterization of global stratospheric sulfate aerosols released by Tonga volcano. *Journal of Quantitative Spectroscopy and Radiative Transfer*, *299*, 108520. https://doi.org/10.1016/j.jqsrt.2023.108520

Biermann, U. M., Luo, B. P., & Peter, T. (2000). Absorption spectra and optical constants of binary and ternary solutions of H2SO4, HNO3, and H2O in the mid infrared at atmospheric temperatures, *104*, 783–793. https://doi.org/10.1021/jp992349i

Bluth, G. J. S., Doiron, S. D., Schnetzler, C. C., Krueger, A. J., & Walter, L. S. (1992). Global tracking of the SO 2 clouds from the June, 1991 Mount Pinatubo eruptions. *Geophysical Research Letters*, *19*(2), 151–154. https://doi.org/10.1029/91GL02792

Boichu, M., Grandin, R., Blarel, L., Torres, B., Derimian, Y., Goloub, P., et al. (2023). *Growth and global persistence of stratospheric sulfate aerosols from the 2022 Hunga Tonga-Hunga Haápai volcanic eruption* (preprint). Preprints. https://doi.org/10.22541/essoar.167631320.00440905/v1

Carn, S. A., Krotkov, N. A., Fisher, B. L., & Li, C. (2022). Out of the blue: Volcanic SO2 emissions during the 2021–2022 eruptions of Hunga Tonga—Hunga Ha'apai (Tonga). *Frontiers in Earth Science*, *10*. Retrieved from https://www.frontiersin.org/articles/10.3389/feart.2022.976962

Carr, J. L., Horváth, Á., Wu, D. L., & Friberg, M. D. (2022). Stereo Plume Height and Motion Retrievals for the Record-Setting Hunga Tonga-Hunga Ha'apai Eruption of 15 January

2022. *Geophysical Research Letters*, *49*(9), e2022GL098131. https://doi.org/10.1029/2022GL098131

Coy, L., Newman, P. A., Wargan, K., Partyka, G., Strahan, S. E., & Pawson, S. (2022). Stratospheric Circulation Changes Associated With the Hunga Tonga-Hunga Ha'apai Eruption. *Geophysical Research Letters*, *49*(22), e2022GL100982. https://doi.org/10.1029/2022GL100982

Dubuisson, P. (2004). Water vapor retrieval over ocean using near-infrared radiometry. *Journal of Geophysical Research*, *109*(D19), D19106. https://doi.org/10.1029/2004JD004516

Dubuisson, P., Buriez, J. C., & Fouquart, Y. (1996). High spectral resolution solar radiative transfer in absorbing and scattering media: Application to the satellite simulation. *Journal of Quantitative Spectroscopy and Radiative Transfer*, *55*(1), 103–126. https://doi.org/10.1016/0022-4073(95)00134-4

Dubuisson, P., Roger, J., Mallet, M., & Dubovik, O. (2006). A Code to Compute the Direct Solar Radiative Forcing: Application to Anthropogenic Aerosols during the Escompte Experiment. In *Proc. International Radiation Symposium (IRS 2004) on Current Problems in Atmospheric Radiation* (pp. 127–130). Busan, Korea: Deepak Publishing, Hampton.

Duflot, V., Bègue, N., Pouliquen, M.-L., Goloub, P., & Metzger, J.-M. (2022). Aerosols on the Tropical Island of La Réunion (21°S, 55°E): Assessment of Climatology, Origin of Variability and Trend. *Remote Sensing*, *14*(19), 4945. https://doi.org/10.3390/rs14194945

Earth and Space Science - 2023 - Wargan - M2-SCREAM A Stratospheric Composition Reanalysis of Aura MLS Data With MERRA-2.pdf. (n.d.).

J. S. Lopes, F., Silva, J. J., Antuña Marrero, J. C., Taha, G., & Landulfo, E. (2019). Synergetic Aerosol Layer Observation After the 2015 Calbuco Volcanic Eruption Event. *Remote Sensing*, *11*(2), 195. https://doi.org/10.3390/rs11020195

Jacquinet-Husson, N., Scott, N. A., Chédin, A., Crépeau, L., Armante, R., Capelle, V., et al. (2008). The GEISA spectroscopic database: Current and future archive for Earth and planetary atmosphere studies. *Journal of Quantitative Spectroscopy and Radiative Transfer*, *109*(6), 1043–1059. https://doi.org/10.1016/j.jqsrt.2007.12.015

Khaykin, S., Podglajen, A., Ploeger, F., Grooß, J.-U., Tence, F., Bekki, S., et al. (2022). Global perturbation of stratospheric water and aerosol burden by Hunga eruption. *Communications Earth & Environment*, *3*(1), 316. https://doi.org/10.1038/s43247-022-00652-x

Klett, J. D. (1985). Lidar inversion with variable backscatter/extinction ratios. *Applied Optics*, *24*(11), 1638–1643. https://doi.org/10.1364/AO.24.001638

Kloss, C., Sellitto, P., Renard, J., Baron, A., Bègue, N., Legras, B., et al. (2022). Aerosol Characterization of the Stratospheric Plume From the Volcanic Eruption at Hunga Tonga 15 January 2022. *Geophysical Research Letters*, *49*(16). https://doi.org/10.1029/2022GL099394

Lac, C., Pichon, A. L., Listowski, C., Abbassi, G., Astafyeva, elvyra, baron, alexandre, et al. (2022). *L'éruption du volcan Hunga Tonga -Hunga Ha'apai le 15 janvier 2022 : un ébranlement du système Terre à l'échelle planétaire*. Zenodo. https://doi.org/10.5281/zenodo.7510334

Lacis, A. A., & Oinas, V. (1991). A description of the correlated *k* distribution method for modeling nongray gaseous absorption, thermal emission, and multiple scattering in

638 vertically inhomogeneous atmospheres. *Journal of Geophysical Research*, *96*(D5), 9027.
639 https://doi.org/10.1029/90JD01945
640 Legras, B., Duchamp, C., Sellitto, P., Podglajen, A., Carboni, E., Siddans, R., et al. (2022). The
641 evolution and dynamics of the Hunga Tonga–Hunga Ha'apai sulfate aerosol plume in the
642 stratosphere. *Atmospheric Chemistry and Physics*, *22*(22), 14957–14970.
643 https://doi.org/10.5194/acp-22-14957-2022
644 Lu, J., Lou, S., Huang, X., Xue, L., Ding, K., Liu, T., et al. (2023). Stratospheric Aerosol and
645 Ozone Responses to the Hunga Tonga-Hunga Ha'apai Volcanic Eruption. *Geophysical*
646 *Research Letters*, *50*(4). https://doi.org/10.1029/2022GL102315
647 Mallet, P.-É., Pujol, O., Brioude, J., Evan, S., & Jensen, A. (2018). Marine aerosol distribution
648 and variability over the pristine Southern Indian Ocean. *Atmospheric Environment*, *182*,
649 17–30. https://doi.org/10.1016/j.atmosenv.2018.03.016
650 Millán, L., Santee, M. L., Lambert, A., Livesey, N. J., Werner, F., Schwartz, M. J., et al. (2022).
651 The Hunga Tonga-Hunga Ha'apai Hydration of the Stratosphere. *Geophysical Research*
652 *Letters*, *49*(13), e2022GL099381. https://doi.org/10.1029/2022GL099381
653 Pitari, G., & Mancini, E. (2002). Short-term climatic impact of the 1991 volcanic eruption of Mt.
654 Pinatubo and effects on atmospheric tracers. *Natural Hazards and Earth System Sciences*,
655 *2*(1/2), 91–108. https://doi.org/10.5194/nhess-2-91-2002
656 Proud, S. R., Prata, A. T., & Schmauß, S. (2022). The January 2022 eruption of Hunga Tonga-
657 Hunga Ha'apai volcano reached the mesosphere. *Science*, *378*(6619), 554–557.
658 https://doi.org/10.1126/science.abo4076
659 Schoeberl, M. R., Wang, Y., Ueyama, R., Taha, G., Jensen, E., & Yu, W. (2022). Analysis and
660 Impact of the Hunga Tonga-Hunga Ha'apai Stratospheric Water Vapor Plume.

Geophysical Research Letters, *49*(20), e2022GL100248. https://doi.org/10.1029/2022GL100248

Schoeberl, Mark R., Jensen, E. J., Pfister, L., Ueyama, R., Avery, M., & Dessler, A. E. (2018). Convective Hydration of the Upper Troposphere and Lower Stratosphere. *Journal of Geophysical Research: Atmospheres*, *123*(9), 4583–4593. https://doi.org/10.1029/2018JD028286

Sellitto, P., Podglajen, A., Belhadji, R., Boichu, M., Carboni, E., Cuesta, J., et al. (2022). The unexpected radiative impact of the Hunga Tonga eruption of 15th January 2022. *Communications Earth & Environment*, *3*(1), 288. https://doi.org/10.1038/s43247-022-00618-z

Sicard, M., Bertolín, S., Mallet, M., Dubuisson, P., & Comerón, A. (2014). Estimation of mineral dust long-wave radiative forcing: sensitivity study to particle properties and application to real cases in the region of Barcelona. *Atmospheric Chemistry and Physics*, *14*(17), 9213–9231. https://doi.org/10.5194/acp-14-9213-2014

Stamnes, K., Tsay, S.-C., Wiscombe, W., & Jayaweera, K. (1988). Numerically stable algorithm for discrete-ordinate-method radiative transfer in multiple scattering and emitting layered media. *Applied Optics*, *27*(12), 2502. https://doi.org/10.1364/AO.27.002502

Taha, G., Loughman, R., Colarco, P. R., Zhu, T., Thomason, L. W., & Jaross, G. (2022). Tracking the 2022 Hunga Tonga-Hunga Ha'apai Aerosol Cloud in the Upper and Middle Stratosphere Using Space-Based Observations. *Geophysical Research Letters*, *49*(19), e2022GL100091. https://doi.org/10.1029/2022GL100091

Taha, Ghassan, Loughman, R., Zhu, T., Thomason, L., Kar, J., Rieger, L., & Bourassa, A. (2021). OMPS LP Version 2.0 multi-wavelength aerosol extinction coefficient retrieval

algorithm. *Atmospheric Measurement Techniques*, *14*(2), 1015–1036. https://doi.org/10.5194/amt-14-1015-2021

Tidiga, M., Berthet, G., Jégou, F., Kloss, C., Bègue, N., Vernier, J.-P., et al. (2022). Variability of the Aerosol Content in the Tropical Lower Stratosphere from 2013 to 2019: Evidence of Volcanic Eruption Impacts. *Atmosphere*, *13*(2), 250. https://doi.org/10.3390/atmos13020250

Tie, X., & Brasseur, G. (1995). The response of stratospheric ozone to volcanic eruptions: Sensitivity to atmospheric chlorine loading. *Geophysical Research Letters*, *22*(22), 3035–3038. https://doi.org/10.1029/95GL03057

Vömel, H., Evan, S., & Tully, M. (2022). Water vapor injection into the stratosphere by Hunga Tonga-Hunga Ha'apai. *Science*, *377*(6613), 1444–1447. https://doi.org/10.1126/science.abq2299

Wang, X., Randel, W., Zhu, Y., Tilmes, S., Starr, J., Yu, W., et al. (2022). Stratospheric climate anomalies and ozone loss caused by the Hunga Tonga volcanic eruption. https://doi.org/10.1002/essoar.10512922.1

Zhou, D. K., Larar, A. M., & Liu, X. (2013). MetOp-A/IASI Observed Continental Thermal IR Emissivity Variations. *IEEE Journal of Selected Topics in Applied Earth Observations and Remote Sensing*, *6*(3), 1156–1162. https://doi.org/10.1109/JSTARS.2013.2238892

Zhu, Y., Bardeen, C. G., Tilmes, S., Mills, M. J., Wang, X., Harvey, V. L., et al. (2022). Perturbations in stratospheric aerosol evolution due to the water-rich plume of the 2022 Hunga-Tonga eruption. *Communications Earth & Environment*, *3*(1), 1–7. https://doi.org/10.1038/s43247-022-00580-w

706 Zuo, M., Zhou, T., Man, W., Chen, X., Liu, J., Liu, F., & Gao, C. (2022). Volcanoes and
707 Climate: Sizing up the Impact of the Recent Hunga Tonga-Hunga Ha'apai Volcanic
708 Eruption from a Historical Perspective. *Advances in Atmospheric Sciences*.
709 https://doi.org/10.1007/s00376-022-2034-1
710